Characterization of Ruthenium Oxide Nanocluster as a Cocatalyst with $(Ga_{1-x}Zn_x)(N_{1-x}O_x)$ for Photocatalytic Overall Water Splitting

Kentaro Teramura,[†] Kazuhiko Maeda,[†] Takafumi Saito,[†] Tsuyoshi Takata,[†] Nobuo Saito,[‡] Yasunobu Inoue,[‡] and Kazunari Domen*[,†]

Department of Chemical System Engineering, School of Engineering, The University of Tokyo, 7-3-1 Hongo, Bunkyo-ku, Tokyo 113-8656, Japan, and Department of Chemistry, Nagaoka University of Technology, 1603-1 Kamitomioka, Nagaoka 940-2188, Japan

Received: August 4, 2005; In Final Form: September 16, 2005

The formation and structural characteristics of Ru species applied as a cocatalyst on $(Ga_{1-x}Zn_x)(N_{1-x}O_x)$ are examined by scanning electron microscopy, X-ray photoelectron spectroscopy, and X-ray absorption spectroscopy. RuO_2 is an effective cocatalyst that enhances the activity of $(Ga_{1-x}Zn_x)(N_{1-x}O_x)$ for overall water splitting under visible-light irradiation. The highest photocatalytic activity is obtained for a sample loaded with 5.0 wt % RuO_2 from an $Ru_3(CO)_{12}$ precursor followed by calcination at 623 K. Calcination is shown to cause the decomposition of initial $Ru_3(CO)_{12}$ on the $(Ga_{1-x}Zn_x)(N_{1-x}O_x)$ surface (373 K) to form Ru(IV) species (423 K). Amorphous RuO_2 nanoclusters are then formed by an agglomeration of finer particles (523 K), and the nanoclusters finally crystallize (623 K) to provide the highest catalytic activity. The enhancement of catalytic activity by Ru loading from $Ru_3(CO)_{12}$ is thus shown to be dependent on the formation of crystalline RuO_2 nanoparticles with optimal size and coverage.

Introduction

Overall water splitting using a heterogeneous photocatalyst is an attractive means of generating "clean" and "renewable" hydrogen. Most existing photocatalysts of this type require modification to facilitate H_2 evolution, typically by loading NiO or RuO_2 as a cocatalyst. However, while these cocatalysts assist H_2 evolution, they do not promote the reverse reaction from H_2 and O_2. NiO-loaded $SrTiO_3$ has been reported to be effective for achieving stoichiometric H_2 and O_2 evolution, and the structure of this catalyst has been studied in detail.[1−5] Many other Ni- and/or NiO-modified photocatalysts, such as $K_4Nb_6O_{17}$,[6,7] $K_2La_2Ti_3O_{10}$,[8,9] and $NaTaO_3$,[10−14] have since been shown to decompose H_2O stoichiometrically into H_2 and O_2 under ultraviolet irradiation.

RuO_2 has also been examined as a cocatalyst for overall water splitting. RuO_2 is well-known as a good oxidation catalyst for O_2 evolution. In the case of water splitting, RuO_2 has been demonstrated by many researchers to be effective as an oxidation site for the evolution of O_2 gas.[15−22] However, Amouyal et al. also revealed that RuO_2 enhances H_2 evolution in the presence of $Ru(bipy)_3^{2+}$, MV^{2+}, and EDTA.[23,24] Sakata et al. reported that the rate of H_2 evolution for the photoreduction of H^+ to H_2 in the presence of ethanol is 30 times higher over RuO_2/TiO_2 than over TiO_2 alone.[25] RuO_2 on n-type semiconductors such as TiO_2 and CdS thus appears to act as a reduction catalyst for H_2 evolution.

Inoue et al. have applied RuO_2 for overall water splitting[26−42] as a cocatalyst with $BaTi_4O_9$, $Ba_6Ti_{17}O_{40}$, $Ba_4Ti_{13}O_{30}$ and $Ba_2Ti_9O_{20}$. The use of $RuCl_3$-derived RuO_2 with $BaTi_4O_9$ resulted in high activity for overall water splitting, despite metallic Ru species themselves being poor cocatalysts.[29,31,34] In those studies, X-ray photoelectron spectroscopy (XPS) and transmission electron microscopy (TEM) analyses revealed that the active Ru sites in these catalysts are well dispersed as RuO_2 species fixed in $BiTi_4O_9$ "nests" (1.4−3.0 nm). It was suggested that the pentagonal-prism tunnel structure of $BaTi_4O_9$ prevents mobilization of the RuO_2 particles from these aggregates. $Ru_3(CO)_{12}$ was found to be a superior precursor to $RuCl_3$ by achieving better dispersion of RuO_2. Accordingly, it appears to be important to achieve a good dispersion of Ru species on photocatalysts such as $Na_2Ti_3O_7$ to obtain high activity. Recently, Inoue et al. discovered that various p-block metal oxides modified with RuO_2 are also effective photocatalysts for overall water splitting.[35−41]

Some (oxy)nitrides, such as TaON,[43,44] Ta_3N_5,[45−47] $MTaO_2N$ (M = Ca, Sr, Ba), $LaTaON_2$,[48,49] and $LaTiO_2N$,[50,51] are potential candidates for visible-light-driven photocatalysts of overall water splitting. In the case of TaON, H_2 evolution under visible-light irradiation in an aqueous methanol solution is enhanced by the photodeposition of Ru particles.[44] Li et al. also reported that the loading of $Y_2Ta_2O_5N_2$ with both Pt and Ru is effective for H_2 evolution.[52] More recently, RuO_2-loaded β-Ge_3N_4 has been reported as the first non-oxide photocatalyst for overall water splitting.[42]

RuO_2 has thus been demonstrated to be important for promoting overall water splitting. In this study, the detailed formation and structure of RuO_2 is examined as a cocatalyst on $(Ga_{1-x}Zn_x)(N_{1-x}O_x)$, which has been shown to be an effective photocatalyst for overall water splitting under visible-light irradiation.[53,54]

Experimental Section

Synthesis of Materials. A mixture of Ga_2O_3 (High Purity Chemicals; 99.9%) and ZnO (Kanto Chemicals; 99%) powders (molecular ratio Ga_2O_3:ZnO = 1:2) was nitrided at 1123 K for

* Corresponding author. Telephone: +81-3-5841-1148. Fax: +81-3-5841-8838. E-mail: domen@chemsys.t.u-tokyo.ac.jp.
[†] The University of Tokyo.
[‡] Nagaoka University of Technology.

10.1021/jp054313y CCC: $30.25
Published on Web 10/21/2005

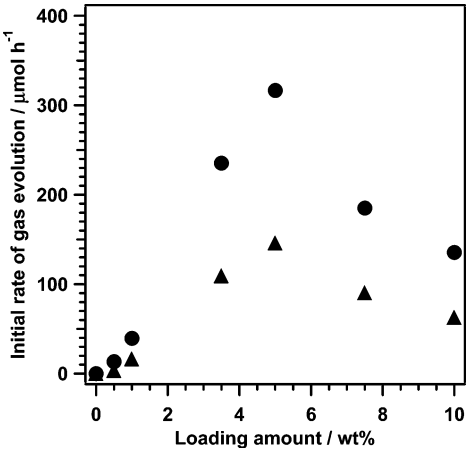

Figure 1. Initial rates of H_2 (circle) and O_2 (triangle) evolution in overall water splitting over $(Ga_{1-x}Zn_x)(N_{1-x}O_x)$ prepared with various loadings of RuO_2 and a common calcination temperature of 673 K.

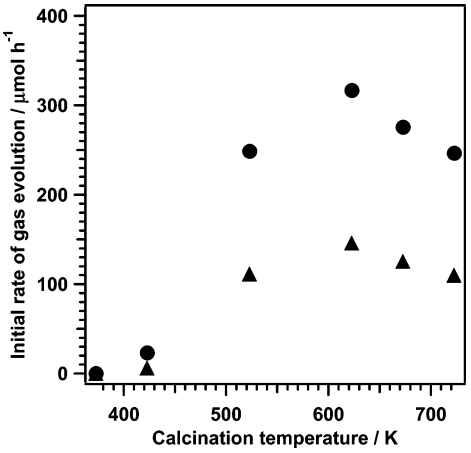

Figure 2. Initial rates of H_2 (circle) and O_2 (triangle) evolution in overall water splitting over 5.0 wt % RuO_2-loaded $(Ga_{1-x}Zn_x)(N_{1-x}O_x)$ after calcination at various temperatures.

15 h under a 250 cm^3 min^{-1} flow of NH_3. After nitridation, the sample was cooled to room temperature under NH_3 flow. The product, $(Ga_{1-x}Zn_x)(N_{1-x}O_x)$, was then loaded with RuO_2 by impregnation from a tetrahydrofuran (THF) solution of triruthenium dodecacarbonyl ($Ru_3(CO)_{12}$) at 333 K for 5 h. The samples were finally evaporated to dryness and calcined at 323, 373, 423, 523, 623, 673, or 723 K for 1 h. One set of samples was not calcined.

Photocatalytic Reaction. Photocatalytic reactions were carried out in an internal-irradiation Pyrex reaction vessel connected to a closed gas circulation and evacuation system. Overall water splitting was examined using an aqueous solution (400 mL) containing 0.30 g of the $RuO_2/(Ga_{1-x}Zn_x)(N_{1-x}O_x)$ powder. The reaction vessel was first evacuated several times to remove air, then irradiated using a 450 W high-pressure Hg lamp (USHIO INC. UM-452) ($\lambda > 300$ nm). It is considered that emission of a high-pressure mercury lamp at 365 and 436 nm mainly contributes to the reaction. The evolved gas was analyzed by TCD gas chromatograph (GC-8A, Shimadzu; stainless steel column, Molecular Sieve-5A).

Characterization of Photocatalyst. X-ray powder diffraction (XRD) patterns were obtained on a Rigaku RINT-UltimaIII Bragg−Brentano-type X-ray diffractometer equipped with a sealed Cu Kα X-ray tube and scintillation counter. Scanning electron microscopy (SEM) images were obtained on a Hitachi S-4700 scanning electron microscope. X-ray photoelectron spectra were captured on a Shimadzu ESCA-3200 spectrometer using Mg Kα radiation. The binding energy of Ru $3p_{3/2}$ peaks is normalized against the $Au4f_{7/2}$ peak measured at the same time. Ru−K edge X-ray absorption fine structure (XAFS) measurements were made at the BL01B1 beamline of the SPring-8 synchrotron facility (Hyogo, Japan) using a ring energy of 8 GeV and stored current from 100 mA in top-up mode (proposal No. 2004B0075−NXa-np). The X-ray absorption spectra were measured in transmission mode at room temperature with a Si(111) two-crystal monochromator. Data reduction was performed using the REX2000 program (Rigaku Corporation). Fourier transformation of the EXAFS spectra in the 4.2−14.7 Å region was performed to obtain the radial structure function (RSF).

Results

Figure 1 shows the dependence of the initial rates of H_2 and O_2 evolution on the loading of RuO_2 for samples calcined at 623 K after impregnation from $Ru_3(CO)_{12}$. No appreciable evolution was observed at RuO_2 loadings of less than 1.5 wt %, above which H_2 and O_2 evolution increased with RuO_2 loading to a maximum at 5.0 wt % RuO_2.

Figure 2 shows the dependence of the initial evolution rate on the calcination temperature for the 5 wt % RuO_2 composition. The catalysts prepared without calcination or with calcination at temperatures below 423 K did not produce appreciable conversion. Starting at 423 K, however, the activity increased markedly with calcination temperature to a maximum at 623 K.

The formation of Ru species on the $(Ga_{1-x}Zn_x)(N_{1-x}O_x)$ catalyst can be determined from the SEM images of various catalyst compositions prepared at the optimal calcination temperature of 623 K (Figure 3). All samples exhibited a distribution of fine secondary particles, which were confirmed by energy-dispersive X-ray (EDX) analysis to be Ru species in all cases. Clusters of smaller than 30 nm in size were observed at RuO_2 loadings of up to 7.5 wt %. At this 7.5 wt % RuO_2 composition, the fine particles almost completely cover the $(Ga_{1-x}Zn_x)(N_{1-x}O_x)$ surface, while at 5.0 wt % RuO_2 or less, the surface is only partially covered with individual fine particles. In the 10 wt % RuO_2 sample, the fine particles form overlapping agglomerates that completely conceal the $(Ga_{1-x}Zn_x)(N_{1-x}O_x)$ surface.

Figure 4 shows SEM images of the 5.0 wt % RuO_2 composition after calcination at various temperatures. The sample calcined at 373 K exhibited a small number of larger agglomerates of Ru species on the catalyst surface. Calcination at 423 K produced a more uniform distribution of fine particles of less than 10 nm in size. The size of fine particles increased with calcination temperature to approximately 30 nm after treatment at 523 and 623 K. At the highest calcination temperature, 723 K, large agglomerates of Ru species began to appear.

Figure 5 shows the Ru 3p X-ray photoelectron spectra for 5.0 wt % RuO_2 samples calcined at 423−723 K. Although the Ru 3d photoelectron signal is much stronger than the Ru 3p photoelectron signal in these samples, the Ru 3d photoelectron signal is obscured by the Ga and Zn Auger photoelectron signals. The Ru $3p_{3/2}$ photoelectron signal can be seen to shift to lower energy with increasing calcination temperature, from 463.7 eV at 423 K to 462.3 eV at 623−723K. The latter is consistent with the binding energy of Ru(IV) in RuO_2. It is known that the binding energy of Ru(0) species coordinated with various ligands appears at higher binding energy than for Ru(IV) in

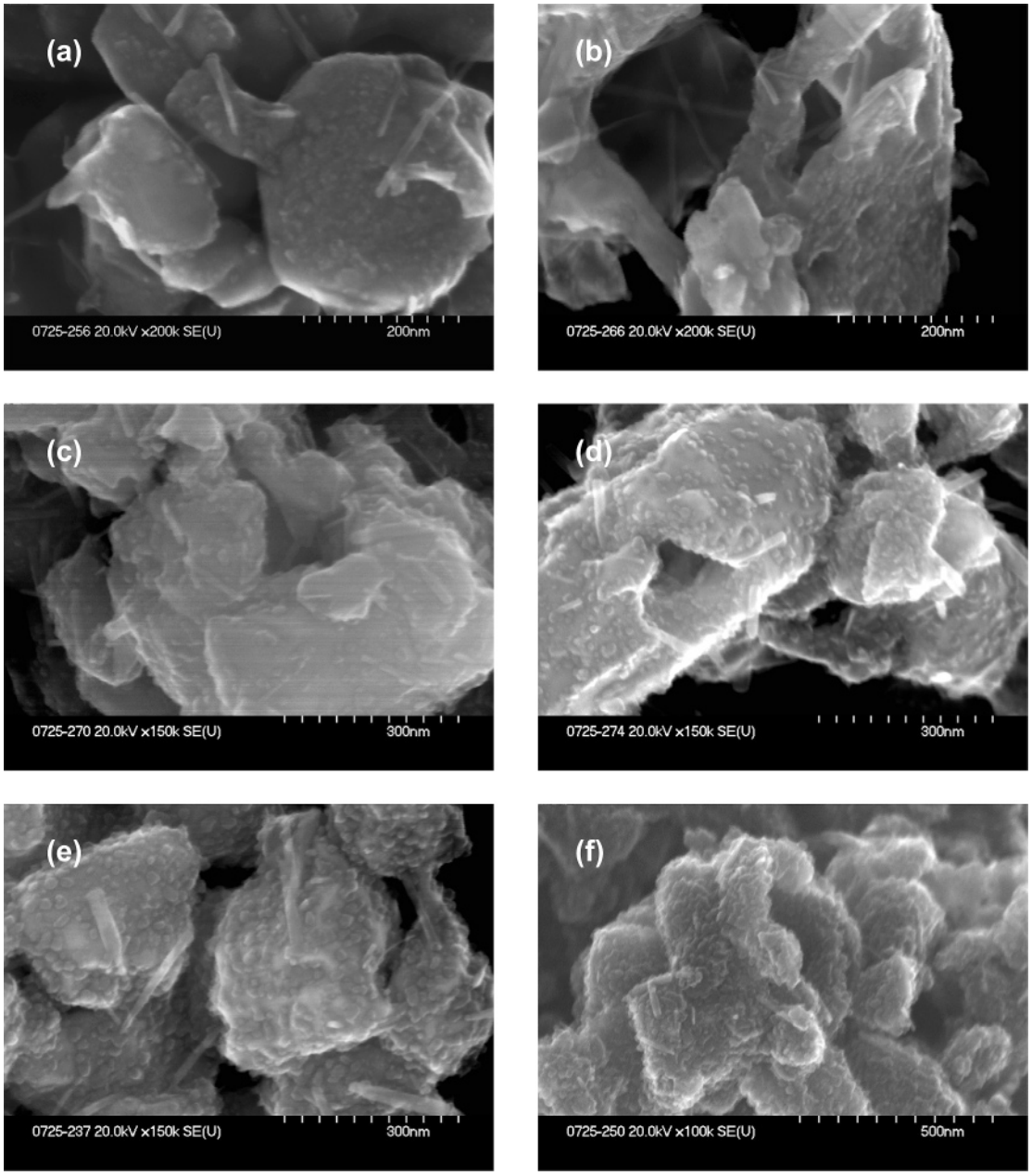

Figure 3. SEM images of $(Ga_{1-x}Zn_x)(N_{1-x}O_x)$ loaded with (a) 0.5, (b) 1.0, (c) 3.5, (d) 5.0, (e) 7.5, and (f) 10.0 wt % RuO_2 followed by calcination at 673 K.

RuO_2. Sham et al. reported that the binding energy of $Ru_3(CO)_{12}$ is higher than that of Ru metal in Ru 3d X-ray photoelectron spectra,[55] consistent with subsequent reports of $Ru_3(CO)_{12}$ on TiO_2(110) based on X-ray photoelectron spectroscopy and temperature-programmed desorption.[56] The position of the Ru $3p_{3/2}$ photoelectron signal for the 5.0 wt % RuO_2 sample calcined at 423 K indicates that some fraction of $Ru_3(CO)_{12}$ or carbonyl species derived from $Ru_3(CO)_{12}$ remain on the surface after heating at this temperature.

Figure 6 shows the Ru−K edge X-ray absorption near-edge structure (XANES) spectra of various catalyst compositions and a common calcination temperature of 623 K. The spectrum for RuO_2 is shown as a reference. The absorption edges of all spectra are identical, indicating that all samples consist of Ru(IV) species. The spectra for all samples are consistent with that for the RuO_2 reference and the corresponding X-ray photoelectron spectra.

Figure 7 shows Fourier transforms of the k^3-weighted Ru−K edge EXAFS spectra of various catalyst compositions calcined at 623 K. The first shell appearing at 1.1−2.0 Å is attributable to the Ru−O configuration, while the second shells (2.2−4.0 Å) are assignable to Ru−(O)−Ru and Ru−(O)−Ga or Zn configuration derived from $(Ga_{1-x}Zn_x)(N_{1-x}O_x)$. The RSF of the 10.0 wt % RuO_2 sample is consistent with that of the RuO_2 reference, whereas the 0.5−7.5 wt % RuO_2 catalysts exhibit shells with shorter distances. It is known that the shell peak in RSF shifts to shorter distances as the particle size decreases. Chen et al. reported the influence of TiO_2 particle size on the XAFS spectra.[57,58] In the present case, Ru(IV) species in the 0.5−7.5 wt % RuO_2 samples are assignable as RuO_2 nanoclusters according to Chen's classification.

Figure 8 shows the Ru−K edge XANES spectra of 5.0 wt % RuO_2 samples calcined at various temperatures. The XANES spectra of the noncalcined sample and the sample calcined at 323 K are comparable with that of the $Ru_3(CO)_{12}$ precursor. The XANES spectrum of the 373 K sample exhibits slight differences, while that for the 423 K sample is distinctly different from the precursor spectrum. The XANES spectra of the samples

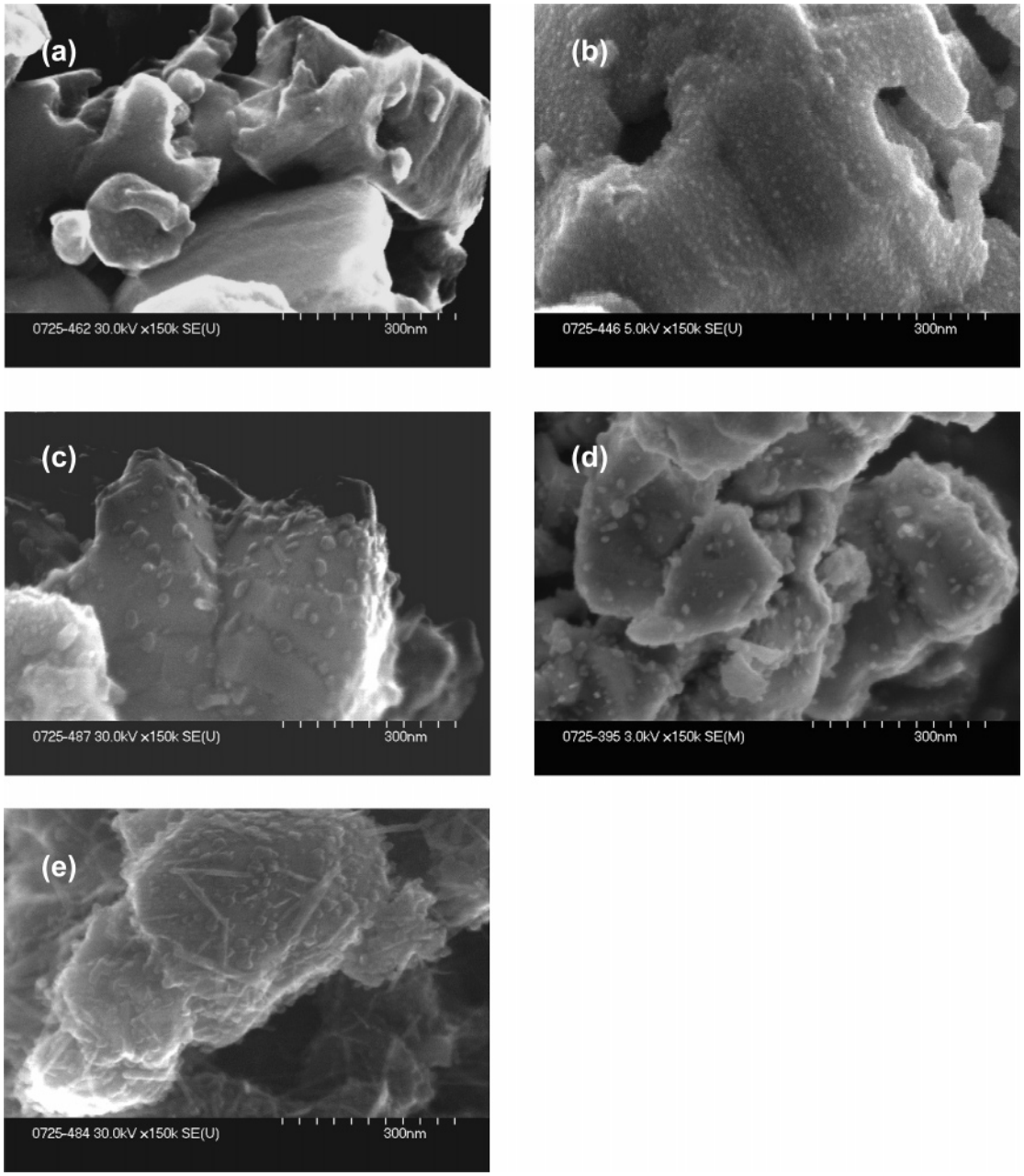

Figure 4. SEM images of 5.0 wt % RuO_2-loaded $(Ga_{1-x}Zn_x)(N_{1-x}O_x)$ (a) as prepared, and (b−e) after calcination at (b) 423, (c) 523, (d) 623, and (e) 723 K.

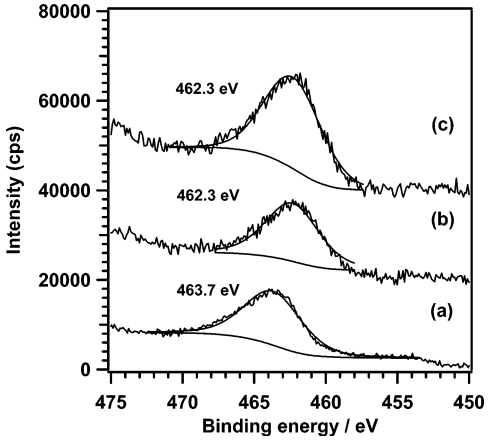

Figure 5. X-ray photoelectron spectra for 5.0 wt % RuO_2-loaded $(Ga_{1-x}Zn_x)(N_{1-x}O_x)$ after calcination at (a) 423, (b) 623, and (c) 723 K.

calcined at 523−723 K are clearly identical to that of Ru(IV) in RuO_2. These results indicate that $Ru_3(CO)_{12}$ on the $(Ga_{1-x}Zn_x)(N_{1-x}O_x)$ surface was decomposed by heating at 373 K, and complete conversion to Ru(IV) species was achieved by calcination at 523 K.

Figure 9 shows Fourier transforms of the k^3-weighted Ru−K edge EXAFS spectra for the 5.0 wt % RuO_2 catalyst composition after calcination at various temperatures. The three characteristic peaks for $Ru_3(CO)_{12}$ in the 1.0−3.0 Å range can be seen in the RSFs of the noncalcined sample and the sample calcined at 323 K, although interaction between $Ru_3(CO)_{12}$ and $(Ga_{1-x}Zn_x)$-$(N_{1-x}O_x)$ appears to influence the spectra to some extent. These results suggest that the $Ru_3(CO)_{12}$ structure persisted when heated at 323 K or below. However, the RSF of the 373 K sample does not include the three characteristic peaks of Ru_3-$(CO)_{12}$, indicating that treatment at this temperature caused the $Ru_3(CO)_{12}$ to collapse. This result is consistent with that from the Ru−K edge XANES spectra (Figure 8). The first shell

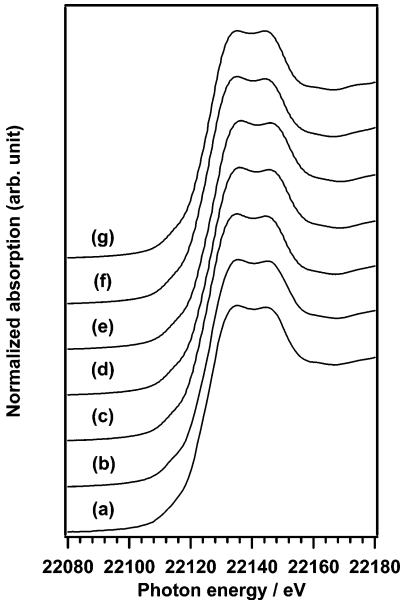

Figure 6. Ru−K edge XANES spectra for $(Ga_{1-x}Zn_x)(N_{1-x}O_x)$ loaded with (a) 0.5, (b) 1.0, (c) 3.5, (d) 5.0, (e) 7.5, and (f) 10.0 wt % RuO_2. (g) Spectrum of RuO_2 as a reference compound.

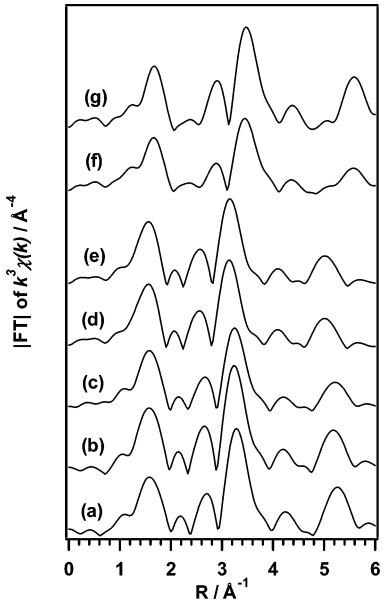

Figure 7. Fourier transforms of k^3-weighted Ru−K edge EXAFS spectra for $(Ga_{1-x}Zn_x)(N_{1-x}O_x)$ loaded with (a) 0.5, (b) 1.0, (c) 3.5, (d) 5.0, (e) 7.5, and (f) 10.0 wt % RuO_2. (g) Spectrum of RuO_2 as a reference compound.

assigned to the Ru−O configuration (1.1−2.0 Å) appears in the 423 K sample, and the second shell (2.2−4.0 Å) due to the Ru−(O)−Ru and Ru−(O)−Ga or Zn configurations is observed in the 523 K sample. The RSFs of the 623 and 723 K sample are similar to that for the RuO_2 reference, although appearing at shorter and longer distances, respectively. These results are consistent with the generation of RuO_2 nanoclusters at temperatures of 573 K and above, and agglomeration at 773 K.

Discussion

The results of overall water splitting using the present catalysts indicate that the density of active species reached a maximum at 5.0 wt % RuO_2. In this optimally loaded sample, the active Ru species after calcination at 623 K is assigned to RuO_2 nanoclusters of smaller than 30 nm on the basis of SEM,

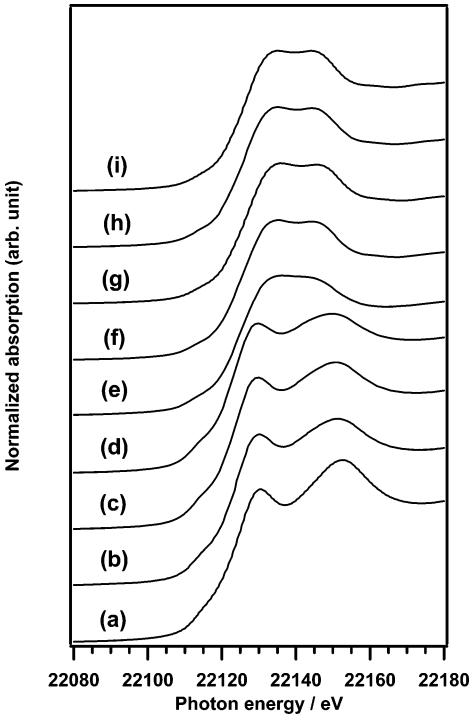

Figure 8. Ru−K edge XANES spectra for 5.0 wt % RuO_2-loaded $(Ga_{1-x}Zn_x)(N_{1-x}O_x)$ (b) as prepared, and (c−h) after calcination at (c) 323, (d) 373, (e) 423, (f) 523, (g) 623, and (h) 723 K. Spectra of (a) $Ru_3(CO)_{12}$ and (i) RuO_2 as reference compounds.

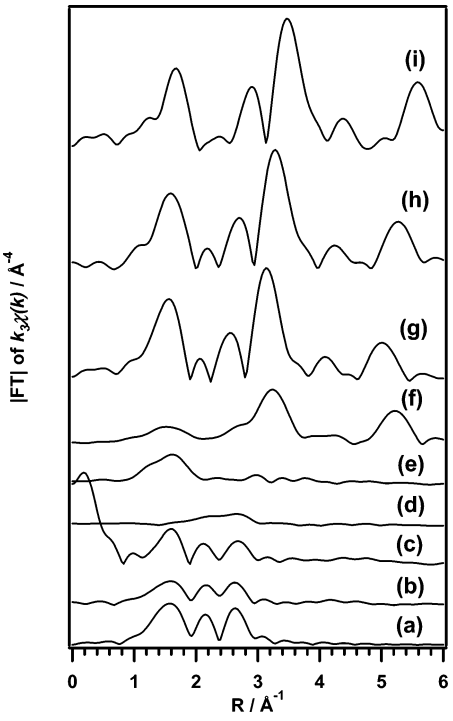

Figure 9. Fourier transforms of k^3-weighted Ru−K edge EXAFS spectra for 5.0 wt % RuO_2-loaded $(Ga_{1-x}Zn_x)(N_{1-x}O_x)$ (b) as prepared, and (c−h) after calcination at (c) 323, (d) 373, (e) 423, (f) 523, (g) 623, and (h) 723 K. Spectra of (a) $Ru_3(CO)_{12}$ and (i) RuO_2 as reference compounds.

XPS, and XAFS analyses. The Fourier transforms of the Ru−K edge EXAFS spectra indicate that RuO_2 nanoclusters were generated by loading with up to 7.5 wt % RuO_2. The SEM image of the 7.5 wt % RuO_2 sample, however, shows that the RuO_2 nanoclusters may have smothered the catalyst surface, thereby lowering the activity for overall water splitting. This is supported

SCHEME 1: Model of Ru Species Structure on $(Ga_{1-x}Zn_x)(N_{1-x}O_x)$ after Calcination at Various Temperatures

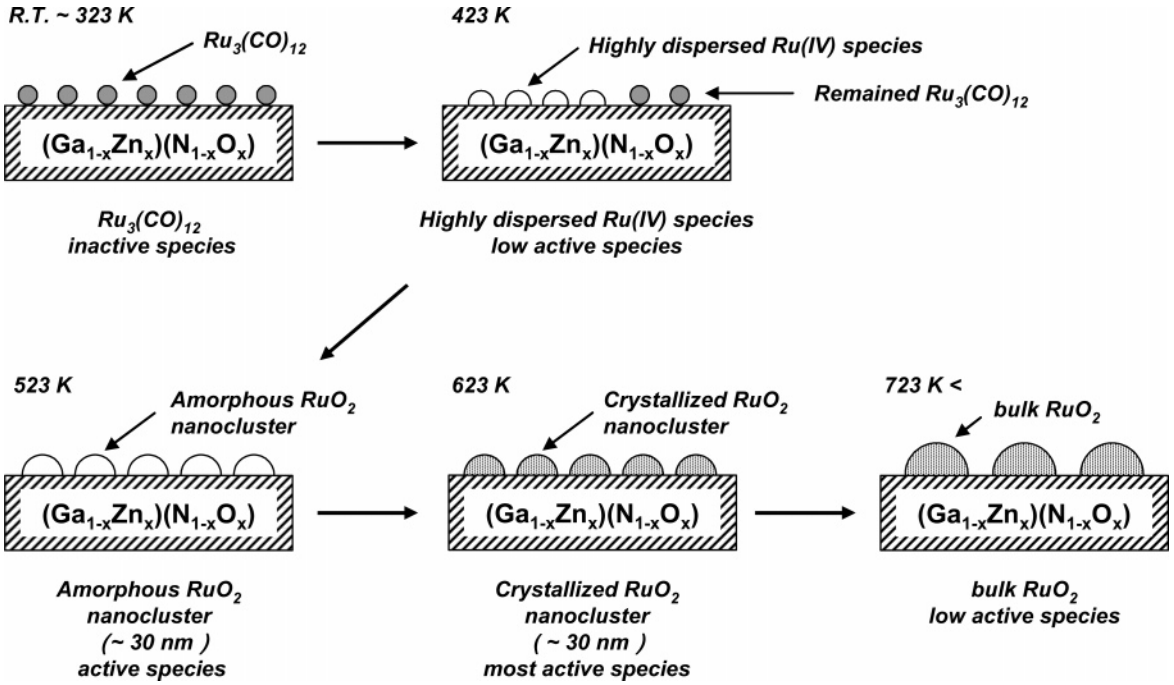

by the very low activity exhibited by the 10.0 wt % RuO_2 catalyst, which was confirmed by SEM to form a thick and overlapping layer of large particles on the catalyst surface. The XAFS spectra indicate that large RuO_2 particles similar to bulk RuO_2 were generated on the surface of this sample. Thus, similar to bulk RuO_2, the loaded particles are less active to promote H_2 evolution. High dispersion of RuO_2 nanoclusters on the catalyst surface is therefore considered to be essential for improving the activity of $(Ga_{1-x}Zn_x)(N_{1-x}O_x)$ for H_2 and O_2 evolution in overall water splitting.

The calcination temperature was found in the present study to be the most important factor in the production of Ru-loaded $(Ga_{1-x}Zn_x)(N_{1-x}O_x)$ with high activity for overall water splitting. Scheme 1 shows a model of the Ru structure on $(Ga_{1-x}Zn_x)(N_{1-x}O_x)$ by impregnation from $Ru_3(CO)_{12}$ followed by calcination at various temperatures. Impregnation results in a distribution of $Ru_3(CO)_{12}$ on the $(Ga_{1-x}Zn_x)(N_{1-x}O_x)$ surface. The XANES and EXAFS results confirmed that this $Ru_3(CO)_{12}$ structure is retained at calcination temperatures of 323 K and below. However, heating at 373 K causes the $Ru_3(CO)_{12}$ structure to partially collapse. Calcination at 423 K produces dramatic changes in the structure of Ru species on the surface. The XANES spectrum of the 423 K sample in fact appears more similar to that for RuO_2. However, the Ru $3p_{3/2}$ peak in the X-ray photoelectron spectrum occurs at 463.7 eV, slightly higher than that for Ru(IV) in RuO_2, indicating that some $Ru_3(CO)_{12}$ persists at this calcination temperature. The observation of a first Ru−O shell peak and weak second Ru−(O)−Ru shell peak in the RSF of this sample are suggestive of highly dispersed Ru(IV) species. Calcination at higher temperature resulted in the agglomeration of fine Ru(IV) species to form amorphous nanoclusters of 10−30 nm in diameter. This is supported by the emergence of the second Ru−(O)−Ru shell peak in the RSF, and is accompanied by a dramatic increase in the rates of H_2 and O_2 evolution. The production of Ru−(O)−Ru networks is thus considered essential to enhance H_2 evolution and improve the efficiency of the overall water splitting reaction. The crystallization of these nanoclusters at 623 K, as indicated by the Fourier transforms of the EXAFS spectra, resulted in the highest activity for H_2 and O_2 evolution in the present study. The decrease in water splitting efficiency for the samples calcined at 723 K can be attributed to the increased size of crystallized RuO_2 nanoclusters.

Conclusion

Using $Ru_3(CO)_{12}$ as a precursor for Ru loading on $(Ga_{1-x}Zn_x)(N_{1-x}O_x)$ catalyst, it was found that calcination of the loaded catalyst is necessary to form and disperse active Ru(IV) species. Calcination at 423 K forms a high dispersion of fine particles of primarily Ru(IV) composition with some remnant $Ru_3(CO)_{12}$. While Ru(IV) species and bulk RuO_2 exhibit less activity for overall water splitting, the RuO_2 nanoclusters provide an enhancement of H_2 and O_2 evolution as a cocatalyst. The activity of the amorphous nanoclusters formed at 523 K is lower than that of the crystallized nanoclusters generated at 623 K, for which the highest activity for overall water splitting was obtained. The formation of crystalline RuO_2 nanoparticles with optimal size and coverage contributes to the enhancement of the stoichiometric H_2 and O_2 evolution for overall water splitting.

Acknowledgment. The staffs of the SPring-8 synchrotron facility and the Japan Synchrotron Radiation Research Institute (JASRI) are gratefully acknowledged for technical assistance in XAFS measurements. This work was supported under the Core Research for Evolutional Science and Technology (CREST) and Solution Oriented Research for Science and Technology (SORST) programs of the Japan Science and Technology Agency (JST), and by the 21st Century Center of Excellent (COE) program of the Ministry of Education, Culture, Sports, Science, and Technology of Japan.

Note Added after ASAP Publication. Correction was made to the spelling of the third author's name and to the EXAFS spectral region in the Discussion section. This paper was published ASAP on 10/21/05. The corrected version was reposted on 10/31/05.

References and Notes

(1) Domen, K.; Naito, S.; Soma, M.; Onishi, T.; Tamaru, K. *J. Chem. Soc., Chem. Commun.* **1980**, 543.

(2) Domen, K.; Naito, S.; Onishi, T.; Tamaru, K. *Chem. Phys. Lett.* **1982**, *92*, 433.

(3) Domen, K.; Naito, S.; Onishi, T.; Tamaru, K. *J. Phys. Chem.* **1982**, *86*, 3657.

(4) Domen, K.; Kudo, A.; Onishi, T.; Kosugi, N.; Kuroda, H. *J. Phys. Chem.* **1986**, *90*, 292.

(5) Domen, K.; Kudo, A.; Onishi, T. *J. Catal.* **1986**, *102*, 92.

(6) Kudo, A.; Tanaka, A.; Domen, K.; Maruya, K.; Aika, K.; Onishi, T. *J. Catal.* **1988**, *111*, 67.

(7) Kudo, A.; Sayama, K.; Tanaka, A.; Asakura, K.; Domen, K.; Maruya, K.; Onishi, T. *J. Catal.* **1989**, *120*, 337.

(8) Takata, T.; Shinohara, K.; Tanaka, A.; Hara, M.; Kondo, J. N.; Domen, K. *J. Photochem. Photobiol. A: Chem.* **1997**, *106*, 45.

(9) Takata, T.; Furumi, Y.; Shinohara, K.; Tanaka, A.; Hara, M.; Kondo, J. N.; Domen, K. *Chem. Mater.* **1997**, *9*, 1063.

(10) Kato, H.; Kudo, A. *Catal. Lett.* **1999**, *58*, 153.

(11) Kato, H.; Kudo, A. *J. Phys. Chem. B* **2001**, *105*, 4285.

(12) Kato, H.; Kudo, A. *Phys. Chem. Chem. Phys.* **2002**, *4*, 2833.

(13) Kato, H.; Kudo, A. *Catal. Today* **2003**, *78*, 561.

(14) Kato, H.; Asakura, K.; Kudo, A. *J. Am. Chem. Soc.* **2003**, *125*, 3082.

(15) Kalyanasundaram, K.; Gratzel, M. *Angew. Chem., Int. Edit. Engl.* **1979**, *18*, 701.

(16) Kawai, T.; Sakata, T. *Nature (London)* **1980**, *286*, 474.

(17) Kawai, T.; Sakata, T. *Chem. Phys. Lett.* **1980**, *72*, 87.

(18) Kiwi, J.; Borgarello, E.; Pelizzetti, E.; Visca, M.; Gratzel, M. *Angew. Chem., Int. Edit. Engl.* **1980**, *19*, 646.

(19) Borgarello, E.; Kiwi, J.; Pelizzetti, E.; Visca, M.; Gratzel, M. *Nature (London)* **1981**, *289*, 158.

(20) Duonghong, D.; Borgarello, E.; Gratzel, M. *J. Am. Chem. Soc.* **1981**, *103*, 4685.

(21) Blondeel, G.; Harriman, A.; Porter, G.; Urwin, D.; Kiwi, J. *J. Phys. Chem.* **1983**, *87*, 2629.

(22) Kiwi, J.; Gratzel, M.; Blondeel, G. *J. Chem. Soc., Dalton Trans.* **1983**, 2215.

(23) Amouyal, E.; Keller, P.; Moradpour, A. *J. Chem. Soc., Chem. Commun.* **1980**, 1019.

(24) Keller, P.; Moradpour, A.; Amouyal, E. *J. Chem. Soc., Faraday Trans. 1* **1982**, *78*, 3331.

(25) Sakata, T.; Hashimoto, K.; Kawai, T. *J. Phys. Chem.* **1984**, *88*, 5214.

(26) Kohno, M.; Ogura, S.; Inoue, Y. *J. Mater. Chem.* **1996**, *6*, 1921.

(27) Kohno, M.; Ogura, S.; Sato, K.; Inoue, Y. *Chem. Phys. Lett.* **1997**, *267*, 72.

(28) Kohno, M.; Ogura, S.; Sato, K.; Inoue, Y. *J. Chem. Soc., Faraday Trans.* **1997**, *93*, 2433.

(29) Ogura, S.; Kohno, M.; Sato, K.; Inoue, Y. *Appl. Surf. Sci.* **1997**, *121*, 521.

(30) Kohno, M.; Kaneko, T.; Ogura, S.; Sato, K.; Inoue, Y. *J. Chem. Soc., Faraday Trans.* **1998**, *94*, 89.

(31) Ogura, S.; Kohno, M.; Sato, K.; Inoue, Y. *J. Mater. Chem.* **1998**, *8*, 2335.

(32) Kohno, M.; Sato, K.; Inoue, Y. *PCCP Phys. Chem. Chem. Phys.* **1999**, *1*, 179.

(33) Kohno, M.; Ogura, S.; Sato, K.; Inoue, Y. *Chem. Phys. Lett.* **2000**, *319*, 451.

(34) Ogura, S.; Sato, K.; Inoue, Y. *PCCP Phys. Chem. Chem. Phys.* **2000**, *2*, 2449.

(35) Sato, J.; Saito, N.; Nishiyama, H.; Inoue, Y. *Chem. Lett.* **2001**, 868.

(36) Sato, J.; Saito, N.; Nishiyama, H.; Inoue, Y. *J. Phys. Chem. B* **2001**, *105*, 6061.

(37) Sato, J.; Saito, N.; Nishiyama, H.; Inoue, Y. *J. Photochem. Photobiol. A: Chem.* **2002**, *148*, 85.

(38) Sato, J.; Kobayashi, H.; Inoue, Y. *J. Phys. Chem. B* **2003**, *107*, 7970.

(39) Sato, J.; Kobayashi, H.; Saito, N.; Nishiyama, H.; Inoue, Y. *J. Photochem. Photobiol. A: Chem.* **2003**, *158*, 139.

(40) Sato, J.; Saito, N.; Nishiyama, H.; Inoue, Y. *J. Phys. Chem. B* **2003**, *107*, 7965.

(41) Sato, J.; Kobayashi, H.; Ikarashi, K.; Saito, N.; Nishiyama, H.; Inoue, Y. *J. Phys. Chem. B* **2004**, *108*, 4369.

(42) Sato, J.; Saito, N.; Yamada, Y.; Maeda, K.; Takata, T.; Kondo, J. N.; Hara, M.; Kobayashi, H.; Domen, K.; Inoue, Y. *J. Am. Chem. Soc.* **2005**, *127*, 4150.

(43) Hitoki, G.; Takata, T.; Kondo, J. N.; Hara, M.; Kobayashi, H.; Domen, K. *Chem. Commun.* **2002**, 1698.

(44) Hara, M.; Nunoshige, J.; Takata, T.; Kondo, J. N.; Domen, K. *Chem. Commun.* **2003**, 3000.

(45) Hitoki, G.; Ishikawa, A.; Takata, T.; Kondo, J. N.; Hara, M.; Domen, K. *Chem. Lett.* **2002**, 736.

(46) Hara, M.; Hitoki, G.; Takata, T.; Kondo, J. N.; Kobayashi, H.; Domen, K. *Catal. Today* **2003**, *78*, 555.

(47) Hara, M.; Hitoki, G.; Takata, T.; Kondo, J. N.; Kobayashi, H.; Domen, K. Ta_3N_5 and TaON as novel photocatalysts responding to visible light. In *Science and Technology in Catalysis 2002*; Kodansha Ltd.: Tokyo, 2003; Vol. 145; p 169.

(48) Hitoki, G.; Takata, T.; Kondo, J. N.; Hara, M.; Kobayashi, H.; Domen, K. *Electrochemistry* **2002**, *70*, 463.

(49) Yamasita, D.; Takata, T.; Hara, M.; Kondo, J. N.; Domen, K. *Solid State Ion.* **2004**, *172*, 591.

(50) Kasahara, A.; Nukumizu, K.; Takata, T.; Kondo, J. N.; Hara, M.; Kobayashi, H.; Domen, K. *J. Phys. Chem. B* **2003**, *107*, 791.

(51) Kasahara, A.; Nukumizu, K.; Hitoki, G.; Takata, T.; Kondo, J. N.; Hara, M.; Kobayashi, H.; Domen, K. *J. Phys. Chem. A* **2002**, *106*, 6750.

(52) Liu, M. Y.; You, W. S.; Lei, Z. B.; Zhou, G. H.; Yang, J. J.; Wu, G. P.; Ma, G. J.; Luan, G. Y.; Takata, T.; Hara, M.; Domen, K.; Can, L. *Chem. Commun.* **2004**, 2192.

(53) Maeda, K.; Takata, T.; Hara, M.; Saito, N.; Inoue, Y.; Kobayashi, H.; Domen, K. *J. Am. Chem. Soc.* **2005**, *127*, 8286.

(54) Maeda, K.; Teramura, K.; Takata, T.; Hara, M.; Saito, N.; Toda, K.; Inoue, Y.; Kobayashi, H.; Domen, K. *J. Phys. Chem. B* **2005**, in press.

(55) Sham, T. K.; Hrbek, J.; Tan, K. H. *Surf. Sci.* **1990**, *236*, 259.

(56) Zhao, X. Y.; Hrbek, J.; Rodriguez, J. A. *Surf. Sci.* **2005**, *575*, 115.

(57) Chen, L. X.; Rajh, T.; Wang, Z. Y.; Thurnauer, M. C. *J. Phys. Chem. B* **1997**, *101*, 10688.

(58) Chen, L. X.; Rajh, T.; Jager, W.; Nedeljkovic, J.; Thurnauer, M. C. *J. Synchrot. Radiat.* **1999**, *6*, 445.